



Contents lists available at ScienceDirect

Sensors and Actuators: B. Chemical

journal homepage: www.elsevier.com/locate/snb

Brightness-constant solvatochromic dye for ratiometric fluorescent imaging of lipid dynamics in developing zebrafish

Guangying Wang^{a,b,c}, Qinglong Qiao^{a,*}, Ning Xu^{a,c}, Xiang Wang^a, Pengjun Bao^{a,b},
Yinchan Zhang^{a,b}, Xiaogang Liu^d, Zhaochao Xu^{a,c,**}

^a CAS Key Laboratory of Separation Science for Analytical Chemistry, Dalian Institute of Chemical Physics, Chinese Academy of Sciences, Dalian 116023, China

^b University of Chinese Academy of Sciences, Beijing 100049, China

^c School of Chemistry, Dalian University of Technology, 2 Linggong Road, Dalian 116024, China

^d Fluorescence Research Group, Singapore University of Technology and Design, 8 Somapah Road, Singapore 487372, Singapore

ARTICLE INFO

Keywords:

Lipid dynamics

Constant brightness

Ratiometric fluorescent probe

Zebrafish

ABSTRACT

Lipids play a crucial role in the growth and development of organisms. However, the lack of effective chemical tools for lipid imaging has hindered a comprehensive understanding of the dynamic changes in lipid content and types in organisms. Here, we introduce a brightness-constant, lipid droplet-targeting ratiometric fluorescent probe called PAA for visualizing dynamic lipid changes during zebrafish growth and development. PAA was an ultra-stable dimer composed of two carbonylpyrenes. Despite variations in polarity, its absorption spectra, quantum yield and fluorescence brightness remained consistent. However, only fluorescence emission wavelength underwent redshift with increasing polarity. These properties enabled stable lipid imaging throughout the entire live zebrafish and allowed for the identification of lipid polarity using ratiometric fluorescence. Furthermore, PAA revealed changes of lipid composition in developing zebrafish. From 3–5 days post fertilization (dpf), zebrafish with undeveloped digestive organs exhibited a gradual decrease in overall lipid content and a reduction in lipid polarity. Subsequently, as the digestive organs fully developed (6–8 dpf), zebrafish were fed with paramecium, resulting in a gradual increase in overall lipid content and lipid polarity. Moreover, starvation experiments indicated that overall lipid content and polar lipids increased in zebrafish fed with paramecium. The successful application of PAA in visualizing lipid dynamics in zebrafish provides new avenues for studying lipid physiology and pathophysiology in living systems.

1. Introduction

Lipids serve crucial roles in cells, acting as key components of cell membranes, a source of energy and participants in signal transduction pathways [1,2]. Dysfunction in lipid metabolism can contribute to the development of various diseases such as atherosclerosis, diabetes and obesity at the organismal level [3–5]. While significant research has focused on investigating lipid abnormalities as disease triggers at the cellular level, translating these findings directly to organisms remains challenging. Zebrafish has emerged as a mature model organism for studying lipids due to its similarities with humans in gene sequences, shared digestive organs (liver, gallbladder, intestine and pancreas), high optical transparency and rapid external development [6–8]. Researchers

have utilized a variety of analytical methods to study lipids in developing zebrafish, including mass spectrometry (MS), liquid chromatography (LC), gas chromatography (GC) and nuclear magnetic resonance (NMR) [9–12]. However, these techniques often require the disruption of biological samples for sample preparation and can only detect individual lipids, lacking the ability to provide a comprehensive understanding of lipid changes in zebrafish. Therefore, there is an unmet need to visualize and analyze dynamic changes in lipids during zebrafish development [13–16].

Ratiometric fluorescent probes, which respond to local lipid polarity by altering the maximum emission wavelength of fluorescence, hold promise as tools for studying lipids in developing zebrafish [15,16]. In order to accurately analyze the polarity and contents of lipids in

* Corresponding author.

** Corresponding author at: CAS Key Laboratory of Separation Science for Analytical Chemistry, Dalian Institute of Chemical Physics, Chinese Academy of Sciences, Dalian, 116023, China.

E-mail addresses: qqjqiao@dicp.ac.cn (Q. Qiao), zcxu@dicp.ac.cn (Z. Xu).

<https://doi.org/10.1016/j.snb.2024.136155>

Received 7 April 2024; Received in revised form 1 June 2024; Accepted 15 June 2024

Available online 25 June 2024

0925-4005/© 2024 Elsevier B.V. All rights reserved, including those for text and data mining, AI training, and similar technologies.

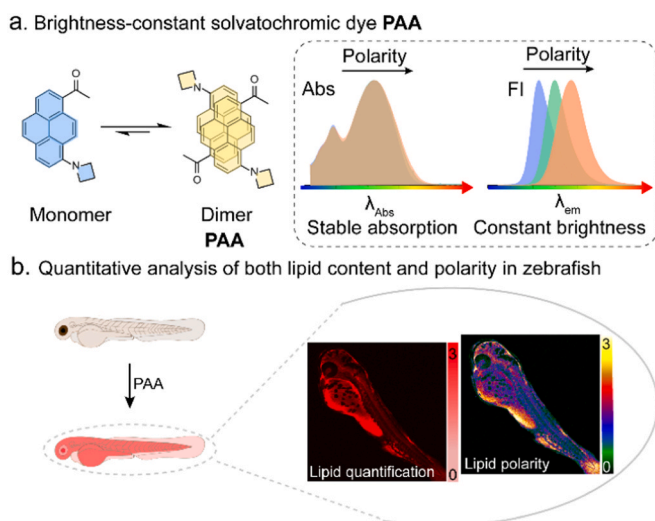
developing zebrafish, fluorescent probes need to be sensitive to lipid polarity, exhibit large Stokes shifts to avoid spontaneous fluorescence interference, and maintain high and stable quantum yields and brightness in different polarity environments, allowing for differential lipid content analysis through fluorescence brightness. Many fluorescent probes targeting lipids have been developed [17–22]. Table S1 listed lipid imaging probes used for zebrafish or other biological tissues, which were less sensitive to polarity [13,23–25]. With increasing polarity, these probes exhibited a slight red shift in fluorescence wavelength. Additionally, they had small Stokes shifts, leading to spontaneous fluorescence interference and reducing image quality. In recent years, researchers have developed many fluorescent probes sensitive to lipid polarity, as shown in Table S2 [26–31]. These probes, such as coumarin derivatives, bodipy derivatives, and commercial lipid probe like Nile Red, were sensitive to lipid polarity. As polarity increased, there was a significant red shift in the fluorescence wavelength. However, the quantum yield and brightness of the reported probes decreased significantly in larger polar environments (Figure S1–S2). As of now, achieving stable quantum yield and brightness for polarity-sensitive probes in lipids of different polarities has been proven to be a challenging task.

In this paper, we introduced a novel polarity-sensitive probe, **PAA**, which exhibited stable quantum yield and brightness in various polarity environments (Scheme 1a). **PAA** emitted fluorescence as a stable dimer, even in well-dissolved solvents. Due to its distinctive molecular configuration as a dimer, **PAA** not only retained the solvatochromic property of traditional polarity-sensitive probes, but also exhibited the following remarkable features: the absorption wavelength and absorbance were hardly affected by polarity (Table S2), and the quantum yield, brightness remained constant in different polarity environments (Figure S1–S2). This unique property enabled sensitive quantitative analysis of both lipid content by fluorescence imaging and lipid polarity by ratiometric imaging in zebrafish (Scheme 1b). Furthermore, **PAA** revealed dynamic changes of lipid content and polarity in developing zebrafish and the effects of paramecium food on zebrafish lipids.

2. Experiment and methods

2.1. General Information

The detailed information regarding the chemical reagents, instruments, synthesis steps and characterization of new compounds, cell culture, and zebrafish culture used in this work was described in the supporting information.



Scheme 1. (a) Brightness-constant solvatochromic dye **PAA**. (b) Quantitative analysis of both lipid content and polarity in zebrafish.

2.2. Computational details

All computations were performed with Gaussian 16 package. The optimized structures of dyes were obtained via density functional theory (DFT) [32]. The computational method was ω B97XD, and the basis set was Def2-SVP. The Gibbs free energy of the monomer and dimer were calculated based on the optimized molecular structures.

2.3. Cell Imaging

Unless otherwise stated, live MCF-7 cells were incubated with different dyes (250 nM) for 0.5 h in an atmosphere of 5 % CO_2 / 95 % air at 37°C. Then the stained cells were imaged without washing. Confocal imaging for lipid droplets colocalization between LD540 and **PAA** was conducted to demonstrated specific labeling of **PAA**. Ex: 405 nm; collected: 450–550 nm for **PAA**. Ex: 543 nm; collected: 560–660 nm for LD540. In ratiometric imaging, lipid droplets were labeled with **PAA**. Ex: 405 nm; collected: 430–510 nm in channel 1 and 510–610 nm in channel 2.

2.4. Zebrafish Imaging

All zebrafish experiments were performed in full compliance with international ethics guidelines. Unless otherwise stated, zebrafish were incubated with dyes (500 nM) for 1 h at room temperature. Then Zebrafish were imaged without washing at room temperature. Zebrafish were incubated for different times with **PAA** or LD493 or Nile Red, the zebrafish were then directly imaged. Ex: 405 nm; collected: 450–550 nm for **PAA**. Ex: 488 nm; collected: 500–600 nm for LD493. Ex: 543 nm; collected: 560–660 nm for Nile Red. In ratiometric imaging experiments, zebrafish were stained with 500 nM **PAA** probe. Ex: 405 nm; collected: 430–510 nm in channel 1 and 510–610 nm in channel 2.

3. Results and discussion

3.1. Dimer configuration and photophysical properties of **PAA**

PAA was synthesized via a two-step reaction (Scheme S1–S3), and its dimeric molecular configuration was confirmed through various analytical techniques including high-resolution mass spectrometry (HRMS), density functional theory (DFT), UV–visible absorption spectroscopy, and fluorescence spectroscopy. Initially, an evident dimer ion peak at 599.2758 [(2 M+H)⁺] (calculated 599.2699, electrospray ionization as the ion source) was observed, providing clear evidence of the stable presence of the **PAA** dimer (Fig. 1a and S4). Utilizing density functional theory, we optimized the ground-state configurations of both the **PAA** monomer and dimer, analyzing their relative Gibbs free energies (Fig. 1b). The results indicated that the relative Gibbs free energy of the **PAA** dimer (-0.57 eV) was lower than that of the monomer (0 eV), suggesting greater stability of the **PAA** dimer over the monomer. Furthermore, examination of the concentration-dependent UV–visible absorption spectra of **PAA** revealed spectral overlap without any isosbestic points (Fig. 1c and S5a). This absence of isosbestic points suggested the presence of a single dimeric species in **PAA** solutions across different concentrations [33]. The inset in Fig. 1c demonstrated a linear increase in absorbance with increasing concentration, further supporting the conclusion. Additionally, the presence of only one fluorescence peak in the spectra confirmed the existence of **PAA** in solution in its dimeric configuration (Fig. 1d, Figure S5b).

We conducted investigations on the UV–visible absorption spectra and fluorescence emission spectra of **PAA** in various solvents (Fig. 1e–f, Table 1). Interestingly, **PAA** exhibited nearly identical peaks at 450 nm in the UV–visible absorption spectra in different solvents, while the fluorescence spectra showed variations. We further analyzed the relationship between the dielectric constant of different solvents and the fluorescence intensity ratio (I_2/I_1) of **PAA**. The results revealed an

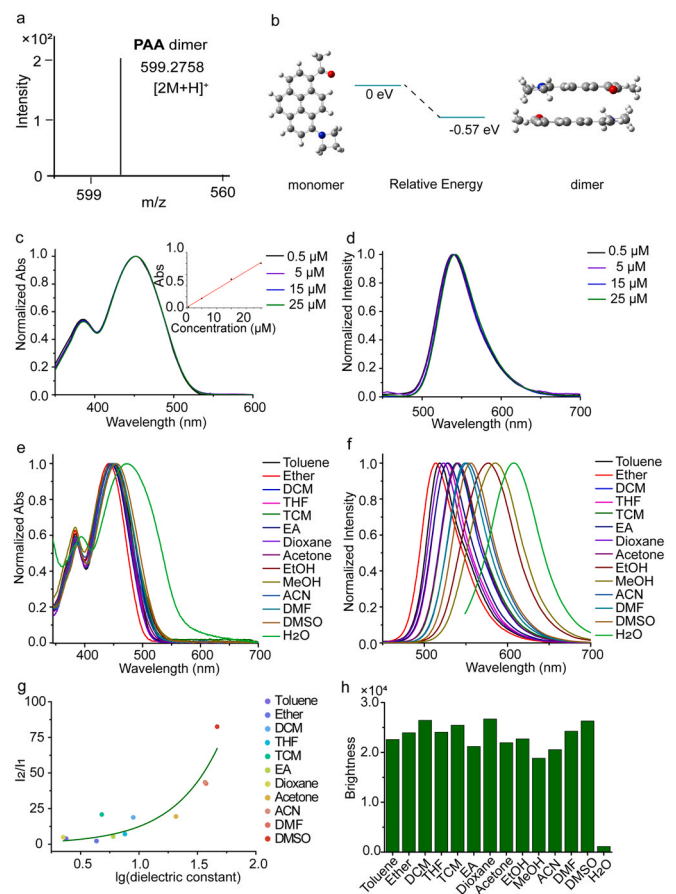


Fig. 1. (a) Structure of PAA. HRMS spectrum of PAA in acetonitrile. (b) Stable monomer and dimer configurations in the ground state of PAA at the ω B97xd/Def2-SVP level in a vacuum. The relative Gibbs free energy of the monomer and dimer were labeled. (c) Normalized absorption spectra of different concentrations of PAA in chloroform. The inset graph illustrated the linear relationship between the concentration and the absorbance of the 452 nm absorption peak. (d) Normalized fluorescence spectra of different concentrations of PAA in chloroform. (e) Normalized absorption spectra of 5 μ M PAA in different solvents. (f) Normalized fluorescence spectra of 5 μ M PAA in different solvents. (g) Relationship diagram between $\lg(\text{dielectric constant})$ and I_2/I_1 . I_2 refers to the integrated area of the fluorescence curve from 510 to 610 nm, and I_1 refers to the integrated area of the fluorescence curve from 430 to 510 nm. (h) Fluorescence brightness of 5 μ M PAA in different solvents.

Table 1
Spectral data of PAA in different solvents.

Solvents	λ_{abs} (nm)	λ_{em} (nm)	$\Delta\lambda$ (nm)	ϵ ($\text{M}^{-1}\text{cm}^{-1}$)	ϕ	Brightness
Toluene	451	518	67	34746	0.65	22574
Ether	441	514	73	34034	0.70	23934
DCM	451	541	90	35022	0.75	26430
THF	448	527	79	35688	0.67	24058
TCM	453	540	87	34082	0.75	25464
EA	444	529	85	34020	0.62	21190
Dioxane	448	524	76	34240	0.78	26710
Acetone	448	540	92	33414	0.66	21956
EtOH	448	577	129	31868	0.71	22716
MeOH	447	587	140	29656	0.64	18832
ACN	446	554	108	31960	0.64	20564
DMF	451	549	98	32670	0.74	24250
DMSO	455	556	101	32596	0.81	26296
H ₂ O	471	606	135	25270	0.04	1126

exponential increase in the fluorescence intensity ratio as the \lg (dielectric constant) of the solvent increased (Fig. 1g). This indicated that PAA was a solvchromic dye that was highly sensitive to polarity, making it suitable as a polarity-sensitive probe. It is worth noting that the quantum yield and brightness

of the reported solvchromic lipid imaging probes decreased significantly as the polarity of the solvent increased (Figure S1-S2). However, The quantum yield and fluorescence brightness of PAA remained constant in different polar environments (Figure S1-S2, Fig. 1h). This characteristic minimized the impact of polarity on fluorescence brightness, thereby enabling more accurate quantification of lipid contents based on PAA fluorescence intensity. Furthermore, PAA exhibited excellent photostability compared with the lipid imaging probe LD493 (Figure S6). Following 8 hours of tungsten lamp irradiation, the fluorescence intensity of PAA gradually decreased to 83 %, whereas that of LD493 decreased significantly to 27 %. Furthermore, PAA showed no influence from pH variations (Figure S7). In summary, PAA exhibited polar sensitivity, constant quantum yield, constant brightness, high photostability, and pH insensitivity, making it a promising candidate as an excellent ratiometric fluorescent probe for lipid imaging.

3.2. Ratiometric imaging of lipid droplets in live cells

Cell imaging experiments demonstrated that PAA selectively stained lipid droplets. MCF-7 cells were treated with PAA and LD540 (a commonly used commercial lipid droplet probe) for 30 minutes. Remarkably, fluorescence between PAA and LD540 exhibited no cross-interference under different excitation wavelengths, enabling co-localized imaging without the need for washing (Fig. 2a). The co-localization of PAA and LD540 was significant, as evidenced by a Pearson correlation coefficient of 0.93 (Fig. 2b). Furthermore, PAA and LD540 showed excellent co-localization in cells treated with oleic acid, with a Pearson correlation coefficient of 0.91 (Fig. 2c-d). These findings

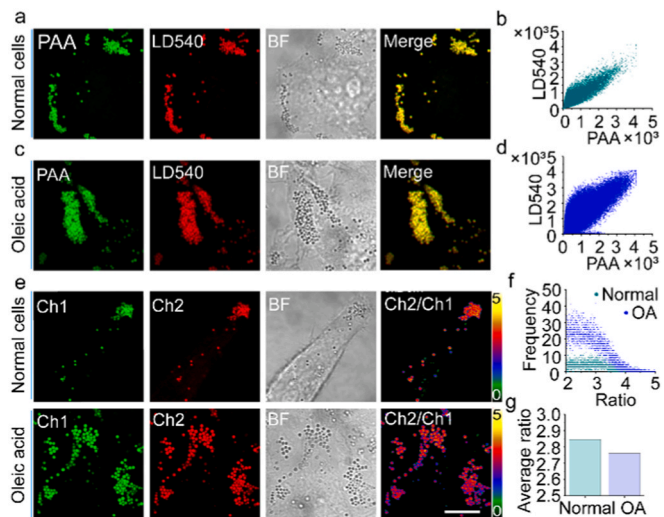


Fig. 2. (a) Confocal imaging of normal MCF-7 cells stained with PAA and commercial dye LD540. (b) Colocalization analysis demonstrating a colocalization coefficient of 0.93 in (a). (c) Confocal imaging of MCF-7 cells treated with 250 μ M oleic acid (OA) for 24 hours, stained with PAA and commercial dye LD540. (d) Colocalization analysis of (c), indicating a colocalization coefficient of 0.91. (e) Ratiometric imaging of MCF-7 cells treated with PAA. One group was normal MCF-7 cells, while the other group was MCF-7 cells incubated with 250 μ M oleic acid for 24 hours. Ch2/Ch1 represents the ratiometric imaging of MCF-7 cells. The collection wavelengths of channel 1 and channel 2 were 430–510 nm and 510–610 nm respectively. (f) Dot plots showing the ratio as a function of the frequency for lipid droplets in (e). (g) The average ratio of lipid droplets in (e). [Dyes] = 250 nM. Scale bar: 10 μ m.

underscored the high specificity of PAA for targeting lipid droplets.

The polarity-dependent chromogenic wavelength of PAA endows it with the ability to discern lipid polarity. By analyzing the fluorescence intensities within the ranges of 430–510 nm and 510–610 nm (Ch2/Ch1), we constructed a ratiometric image, as depicted in Fig. 2e. Further analysis of the distribution and averages about ratiometric values allowed us to quantify lipid polarity changes. Interestingly, the results revealed no significant difference in the ratio of lipid droplets between normal cells and oleic acid-treated cells. The lipid droplets ratio in oleic acid-treated cells (2.76) was marginally lower than that in normal cells (2.85), suggesting that the lipid droplets in oleic acid-treated cells possessed slightly lower polarity compared to those in normal cells. The effect of PAA on cell viability was assessed with the MTT assay. Figure S8 showed that the cell viability at a high concentration of 100 μM PAA for 24 hours was similar to that at low concentrations of 0.1 μM and 0.5 μM , indicating that PAA has minimal impact on cell viability. This was an advantage for monitoring the dynamic changes of lipids in living cells and organisms using PAA.

3.3. Lipid imaging in zebrafish

We subsequently examined the lipid imaging capability of PAA in zebrafish. Zebrafish at 4 days post fertilization (dpf) were immersed in a nutrient solution containing PAA for varying durations and imaged without washing (Fig. 3a). Initially, we observed fluorescence throughout the zebrafish, albeit relatively weak, after 0.5 hours of incubation time. However, the fluorescence intensity throughout the zebrafish markedly increased after 2 hours of incubation time. Subsequently, the fluorescence intensity in zebrafish, except for the

abdominal region, notably decreased since 13 hours and became comparable to background intensity at 48 hours. Analysis of the results

revealed that the fluorescence intensity ratio (F_2/F_1) exhibited an exponential decrease with the extension of incubation time (Fig. 3c). This trend could be attributed to the abundance of lipids in the zebrafish abdomen, leading to the accumulation of PAA in this region after metabolism.

To confirm that PAA accumulated in the abdomen of zebrafish without altering lipid distribution, we conducted a control experiment. Zebrafish were initially incubated with PAA for 2–3 days and subsequently stained with PAA again for 1 hour before imaging (Fig. 3b). Fluorescence was observed throughout the entire zebrafish stained with PAA again before imaging. Further analysis were to assess the average fluorescence intensity between the abdomen and non-abdominal regions of zebrafish. Notably, the non-abdominal fluorescence intensity remained consistent when zebrafish were incubated for 2 or 3 days without a secondary staining before imaging. However, a significant increase in non-abdominal fluorescence intensity was observed when zebrafish were incubated for 2 or 3 days with a secondary staining before imaging. Additionally, the fluorescence intensity in zebrafish incubated for 3 days (6 dpf zebrafish) was stronger than that in zebrafish incubated for 2 days (5 dpf zebrafish). This can be attributed to the increased lipid content in 6 dpf zebrafish fed with paramecia (Fig. 3d). Interestingly, a similar phenomenon was observed with Nile Red and LD493. After metabolism in zebrafish, both Nile Red and LD493 also accumulated in the abdomen, which is rich in lipids (Figure S9). This suggested that the dye was readily metabolized by zebrafish into the lipid-rich abdomen after prolonged incubation. Consequently, we opted to incubate zebrafish with PAA for only 1 hour in subsequent experiments.

3.4. Lipid dynamic imaging in zebrafish growth

0–5 dpf zebrafish rely on the yolk for nutrition. Subsequently, their digestive system matures, and zebrafish start actively feeding after 5 days post fertilization [34–37]. To examine the differences in lipid content and polarity during the development of digestive organs, ratiometric fluorescent imaging was conducted on 3–8 dpf zebrafish treated with PAA (Fig. 4a). This imaging approach allowed visualization of variations in lipid content and polarity throughout the developing zebrafish. High-magnification microscopic imaging of the head and abdomen distinctly revealed localized differences in lipid polarity (Fig. 4a, Figure S10).

Subsequently, we conducted quantitative analysis of the overall lipid content in the developing zebrafish (Fig. 4b, Fig. 4e). The average fluorescence intensity of 3–5 dpf zebrafish exhibited a decreasing trend, indicating a gradual reduction in the overall lipid content. This observation aligned with previous literature reported [34]. The lipid content in 5 dpf zebrafish decreased to 57 % of that in 3 dpf zebrafish. This reduction could be attributed to the fact that zebrafish at this stage relied solely on yolk for nutrition, and part of the lipid consumption may have been utilized for the metabolic processes. The relatively stable average fluorescence intensity observed between 5 and 6 dpf zebrafish indicated that the lipid content remained relatively constant. This stability was likely due to the fact that the energy intake from food (paramecia) balanced the energy expenditure of the 6 dpf zebrafish. Conversely, the average fluorescence intensity of

6–8 dpf zebrafish exhibited an increasing trend, indicating a gradual rise in lipid content. The lipid content of 8 dpf zebrafish increased to 1.72 times that of 5 dpf zebrafish. Fig. 4e succinctly illustrated these results. In summary, the overall lipid content of 3–5 dpf zebrafish gradually decreased before the maturation of the digestive system. After the digestive system matured, the lipid content of 6–8 dpf zebrafish gradually increased.

The ratiometric analysis of whole-body lipids in 3–8 dpf zebrafish further unveiled differences in lipid polarity during the maturation of

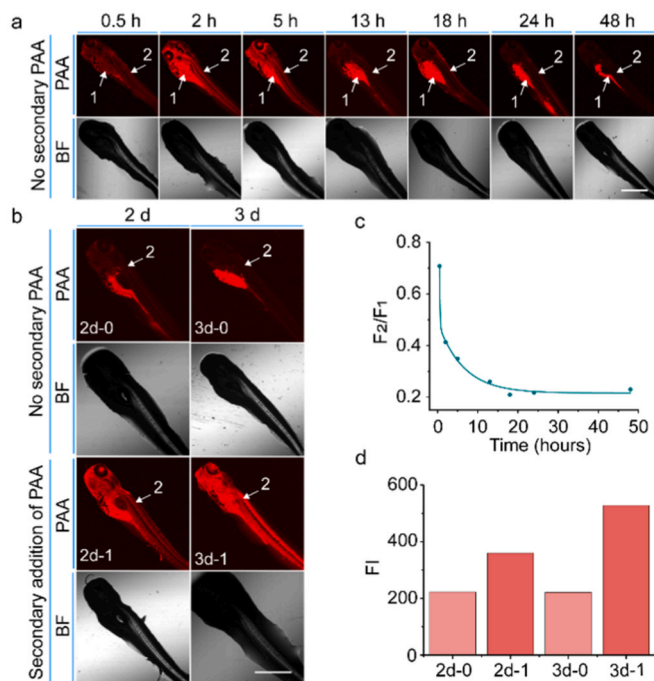


Fig. 3. (a) Confocal imaging of 4 dpf zebrafish treated with PAA for different durations. No additional dye was added before imaging. (b) Two groups of experiments were performed. In one group, PAA was not added twice before imaging. In the other group, 3 dpf zebrafish were incubated with PAA for two or three days and then further incubated with PAA for 1 hour before confocal imaging. (c) Relationship diagram illustrating the correlation between incubation time and F_2/F_1 in (a). Here, F_1 represented the average fluorescence intensity of the yolk, and F_2 represented the average fluorescence intensity of zebrafish excluding the yolk. (d) Changes in average fluorescence intensity of zebrafish excluding the yolk in (b). Confocal imaging of zebrafish were recorded with a 5x/NA 0.10 objective lens. [Dyes] = 500 nM. Scale bar: 800 μm .

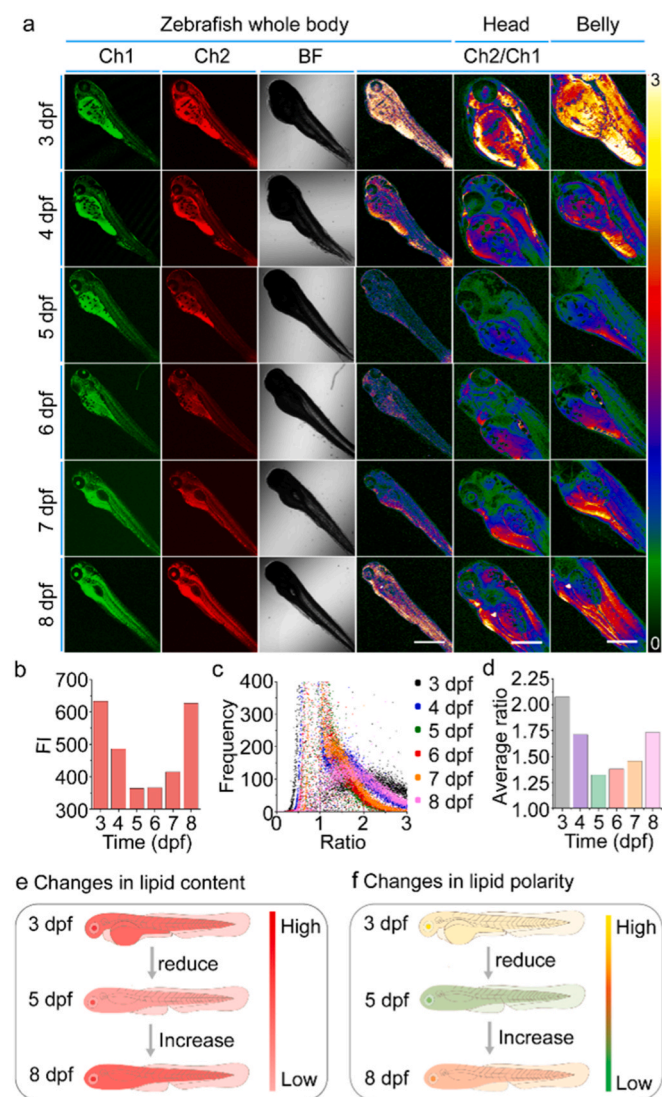


Fig. 4. (a) Ratiometric imaging of different dpf zebrafish treated with PAA. Zebrafish at 6 dpf, 7 dpf, and 8 dpf were fed an appropriate amount of paramecium, while zebrafish at 3 dpf, 4 dpf, and 5 dpf were not fed. The collection wavelengths of channel 1 and channel 2 were 430–510 nm and 510–610 nm respectively. Ch2/Ch1 represented ratiometric imaging. (b) Changes in average fluorescence intensity of different dpf zebrafish as depicted in (a). (c) Ratiometric analysis of different dpf zebrafish as shown in (a). (d) Average ratiometric values of different dpf zebrafish in (c). (e) Model illustrating changes in lipid content of 3–8 dpf zebrafish. (f) Model depicting changes in lipid polarity of 3–8 dpf zebrafish. Confocal images of the whole body, head, and belly was recorded with 5x/NA 0.10, 10x/NA 0.40 and 10x/NA 0.40 objective lens respectively. [Dyes] = 500 nM. Scale bar of the whole body: 800 μ m. Scale bar of head and belly: 400 μ m.

digestive organs. The ratiometric values of whole-body lipids in 3–8 dpf zebrafish generally ranged from 0.5 to 3, with slight variations in frequency for each ratio (Fig. 4c). Notably, larger ratiometric values corresponded to greater lipid polarity. The average ratiometric analysis of 3–8 dpf zebrafish revealed that the average ratiometric values gradually decreased from 3 day to 5 days post-fertilization (dpf), with the ratiometric value at 5 dpf zebrafish declining to 64 % of that at 3 dpf. Conversely, the average ratiometric values gradually increased from 5 to 8 days post fertilization (dpf), with the ratiometric value of 8 dpf zebrafish rising to 1.31 times that of 5 dpf zebrafish (Fig. 4d). The observed pattern of changes in lipid polarity (Fig. 4f), showed a decrease from 3 to 5 dpf, followed by an increase from 5 to 8 dpf. We speculated

that 3–5 dpf zebrafish might consumed lipids with higher polarity, and the overall polar lipid content in 6–8 dpf zebrafish increased after feeding on paramecia, which are rich in polar lipids [38].

3.5. Effects of Paramecium Food on Zebrafish Lipids

The dynamic imaging capability of PAA for lipids enables tracking the growth and development of zebrafish. To illustrate this, we evaluated the influence of paramecia on the lipid profile of developing zebrafish by comparing lipid content differences between those fed with or without paramecium (Fig. 5). The fluorescence intensity of the control zebrafish was significantly higher than that of starved zebrafish, as depicted in Fig. 5a. At 10 dpf, the average fluorescence intensity of the control group (869 a.u.) surpassed that of the starved group (478 a.u.). Similarly, at 12 dpf, the average fluorescence intensity of the control group (1170 a.u.) exceeded that of the starved group (343 a.u.). It's noteworthy that as zebrafish developed, the fluorescence intensity increased in the control group while decreasing in the starved group (Fig. 5b). In conclusion, the lipid content in zebrafish fed with paramecia was greater than that in the starved zebrafish, as shown in Fig. 5e.

Simultaneously, we investigated the impact of paramecium on the lipid polarity of developing zebrafish. The ratio of zebrafish in the

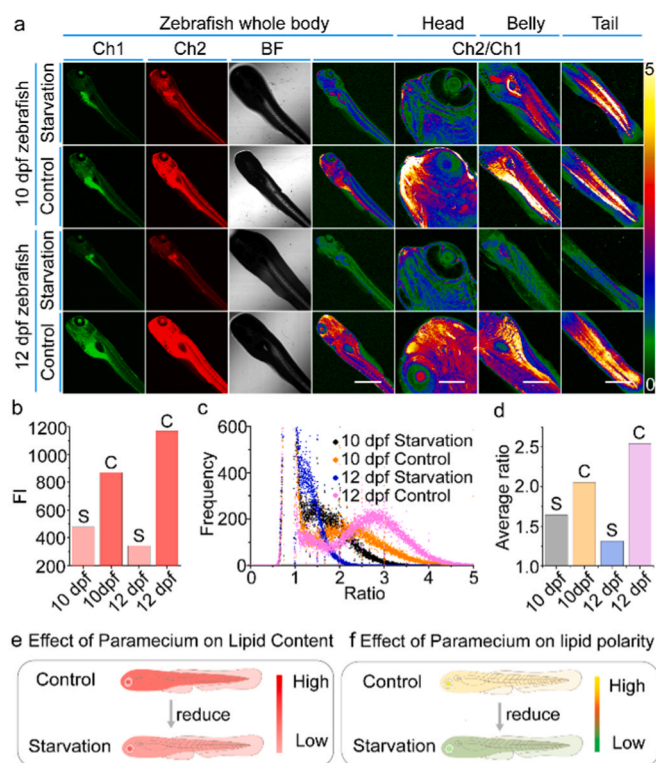


Fig. 5. (a) The starvation experiment: Zebrafish were deprived of food (paramecium) since 9 days post fertilization. The controlled experiment: Zebrafish were fed an appropriate amount of paramecium daily. Ratiometric imaging of 10 dpf and 12 dpf zebrafish treated with PAA were conducted. The collection wavelengths of channel 1 and channel 2 were 430–510 nm and 510–610 nm respectively. Ch2/Ch1 represented ratiometric imaging. (b) Changes in average fluorescence intensity of zebrafish in (a). The starvation experiment was marked as S, and the controlled experiment as C. (c) Dot plots showing the ratio as a function of the frequency for the whole bodies in (a). (d) Average ratiometric analysis for zebrafish in (c). (e) Model depicting the effect of paramecium on the lipid content of zebrafish. (f) Model illustrating the effect of paramecium on the lipid polarity of zebrafish. Confocal images of the whole body, head, belly and tail were recorded with 5x/NA 0.10, 20x/NA 0.75, 10x/NA 0.40 and 10x/NA 0.40 objective lens respectively. [Dyes] = 500 nM. Scale bar of the whole body: 800 μ m. Scale bar of the head: 200 μ m. Scale bar of the belly and tail: 400 μ m.

control group was significantly higher than that of the starved zebrafish (Fig. 5a). High-magnification ratiometric imaging of the head, belly, and tail provided a clearer visualization of the local distribution in zebrafish (Fig. 5a, Figure S11). The ratiometric distribution of 10 dpf and 12 dpf zebrafish indicated consistently higher ratiometric values in the control group compared to the starved group (Fig. 5c). This observation was supported by the analysis of the average ratiometric values (Fig. 5d). Notably, the ratiometric values of zebrafish in the control group increased as they developed, while those of the starved group decreased. These findings were illustrated in Fig. 5f. Zebrafish fed with paramecia exhibited higher lipid polarity compared to starved zebrafish. Since paramecia are rich in polar lipids, the polar lipid content increased after zebrafish ingested them [38].

4. Conclusions

In this work, we introduced a novel ratiometric fluorescent probe for lipids in zebrafish, PAA, based on a stable dimer. It's the first instance of such development. Notably, while the fluorescence emission wavelength varied, the fluorescence brightness remained relatively constant across different polar solvents. The unique property enabled sensitive quantitative analysis of both lipid content and polarity in zebrafish, a capability not achievable with previous fluorescent dyes. Initially, we evaluated the effect of incubation time on the distribution of the dye in live zebrafish. PAA, along with commercial dyes LD493 and Nile Red, exhibited a tendency to accumulate in the lipid-rich abdomen after prolonged incubation and metabolism. Subsequently, an optimal incubation time of 1 hour for PAA was selected for subsequent experiments. We observed content and polarity differences of local lipids in developing zebrafish through fluorescence imaging and ratiometric imaging. To understand lipid change patterns in developing zebrafish, we devised a method converting fluorescence intensity into quantitative lipid content parameters and ratiometric values into quantitative lipid polarity parameters. By quantitatively comparing fluorescence intensity and ratiometric values, variations in lipid content and polarity could be analyzed. When the digestive system of 3–5 dpf zebrafish was not yet fully developed, overall lipid content and polarity gradually decreased. Conversely, as the digestive system of 6–8 dpf zebrafish matured, both lipid content and polarity gradually increased. This trend could be attributed to the ingestion of lipid-rich paramecia, increasing lipid content and polarity. Starvation experiments confirmed that lipid content and polarity increased when zebrafish ingested paramecia. In conclusion, our study underscores the significance of the PAA probe for quantitative assessment of lipid content and polarity in live zebrafish. We believe these findings are crucial for understanding the role of lipids in the development of zebrafish.

CRedit authorship contribution statement

Xiang Wang: Data curation. **Pengjun Bao:** Data curation. **Yinchan Zhang:** Data curation. **Xiaogang Liu:** Formal analysis, Data curation. **Zhaochao Xu:** Writing – review & editing, Writing – original draft, Supervision, Project administration, Funding acquisition, Conceptualization. **Guangying wang:** Writing – original draft, Investigation, Formal analysis, Data curation. **Qinglong Qiao:** Writing – original draft, Supervision, Funding acquisition. **Ning Xu:** Data curation.

Declaration of Competing Interest

The authors declare that they have no known competing financial interests or personal relationships that could have appeared to influence the work reported in this paper.

Data availability

No data was used for the research described in the article.

Acknowledgements

This work is supported by the National Natural Science Foundation of China (22225806, 22078314, 22278394, 22378385) and Dalian Institute of Chemical Physics (DICPI202142, DICPI202436). The authors thank the support from A*STAR under its Advanced Manufacturing and Engineering Program (A2083c0051), the Ministry of Education, Singapore (MOE-MOET2EP10120–0007).

Appendix A. Supporting information

Supplementary data associated with this article can be found in the online version at doi:10.1016/j.snb.2024.136155.

References

- [1] K. Simons, E. Ikonen, Functional rafts in cell membranes, *Nature* 387 (1997) 569–572.
- [2] S. Spiegel, D. Foster, R. Kolesnick, Signal transduction through lipid second messengers, *Curr. Opin. Cell Biol.* 8 (1996) 159–167.
- [3] J.L. Anderson, J.D. Carten, S.A. Farber, Zebrafish lipid metabolism: from mediating early patterning to the metabolism of dietary fat and cholesterol, *Methods Cell Biol.* 101 (2011) 111–141.
- [4] I.B. Dawid, *Developmental Biology of Zebrafish*, *Ann. N. Y. Acad. Sci.* 1038 (2024) 88–93.
- [5] P. Giardoglou, D. Beis, On zebrafish disease models and matters of the heart, *Biomedicines* 7 (2019) 15.
- [6] S. Lange, J.M. Inal, Animal models of human disease, *Int. J. Mol. Sci.* 24 (2023) 15821.
- [7] K.N. Wallace, M. Pack, Unique and conserved aspects of gut development in zebrafish, *Dev. Biol.* 255 (2003) 12–29.
- [8] C.A. MacRae, R.T. Peterson, Zebrafish as tools for drug discovery, *Nat. Rev. Drug. Discov.* 14 (2015) 721–731.
- [9] X. Zhao, J. Chen, W. Zhang, C. Yang, X. Ma, S. Zhang, X. Zhang, Lipid alterations during zebrafish embryogenesis revealed by dynamic mass spectrometry profiling with C=C specificity, *J. Am. Soc. Mass Spectrom.* 30 (2019) 2646–2654.
- [10] W.L. Stutts, M.M. Knuth, M. Ekelöf, D. Mahapatra, S.W. Kullman, D.C. Muddiman, Methods for cryosectioning and mass spectrometry imaging of whole-body zebrafish, *J. Am. Soc. Mass Spectrom.* 31 (2020) 768–772.
- [11] S.M. Huang, F. Xu, S.H. Lam, Z. Gong, C.N. Ong, Metabolomics of developing zebrafish embryos using gas chromatography- and liquid chromatography-mass spectrometry, *Mol. BioSyst.* 9 (2013) 1372.
- [12] Y.F.V. Amerongen, U. Roy, H.P. Spaink, H.J.M.D. Groot, D. Huster, J. Schiller, A. Alia, *Zebrafish* 11 (2014) 240–247.
- [13] J. Chen, W. Liu, X. Fang, Q. Qiao, Z. Xu, BODIPY 493 acts as a bright buffering fluorogenic probe for super-resolution imaging of lipid droplets, *Chin. Chem. Lett.* 33 (2022) 5042–5046.
- [14] Q. Bai, C. Yang, M. Yang, Z. Pei, X. Zhou, J. Liu, H. Ji, G. Li, M. Wu, Y. Qin, Q. Wang, L. Wu, pH-dominated selective imaging of lipid droplets and mitochondria via a polarity-reversible ratiometric fluorescent probe, *Anal. Chem.* 94 (2022) 2901–2911.
- [15] K.N. Wang, L.Y. Liu, D. Mao, S. Xu, C.P. Tan, Q. Cao, W. Mao, B. Liu, A polarity-sensitive ratiometric fluorescence probe for monitoring changes in lipid droplets and nucleus during ferroptosis, *Angew. Chem. Int. Ed.* 60 (2021) 25104–25113.
- [16] H. Tian, A.C. Sedgwick, H.H. Han, S. Sen, G.R. Chen, Y. Zang, J.L. Sessler, T. D. James, J. Li, X.P. He, Fluorescent probes for the imaging of lipid droplets in live cells, *Coord. Chem. Rev.* 427 (2021) 213577.
- [17] N. Li, W. Qin, Y. Chen, K. Liu, S. Wang, F. Kong, Construction of a robust polarity sensitive platform and its application for tracking of lipid droplets decrease under oxidative stress in live cells, *Sens. Actuators B Chem.* 346 (2021) 130491.
- [18] J. Li, Q. Qiao, Y. Ruan, N. Xu, W. Zhou, G. Zhang, J. Yuan, Z. Xu, A fluorogenic probe for SNAP-tag protein based on ESPT ratiometric signals, *Chin. Chem. Lett.* 34 (2023) 108266.
- [19] Y. Zhang, W. Zhou, N. Xu, G. Wang, J. Li, K. An, W. Jiang, X. Zhou, Q. Qiao, X. Jiang, Z. Xu, Aniline as a TICT rotor to derive methine fluorogens for biomolecules: A curcuminoid-BF₂ compound for lighting up HSA/BSA, *Chin. Chem. Lett.* 34 (2023) 107472.
- [20] J. Pan, W. Lin, F. Bao, Q. Qiao, G. Zhang, Y. Lu, Z. Xu, Multiple fluorescence color transitions mediated by anion- π interactions and C-F covalent bond formation, *Chin. Chem. Lett.* 34 (2023) 107519.
- [21] W. Liu, J. Chen, Q. Qiao, X. Liu, Z. Xu, A TICS-fluorophore based probe for dual-color GSH imaging, *Chin. Chem. Lett.* 33 (2022) 4943–4947.
- [22] X. Duan, P. Li, P. Li, T. Xie, F. Yu, B. Tang, The synthesis of polarity-sensitive fluorescent dyes based on the BODIPY chromophore, *Dyes Pigments* 89 (2011) 217–222.
- [23] K. Purevsuren, Y. Shibuta, S. Shiozaki, M. Tsunoda, K. Mizukami, S. Tobita, T. Yoshihara, Blue-emitting lipid droplet probes based on coumarin dye for multi-color imaging of living cells and fatty livers of mice, *J. Photochem. Photobiol. Chem.* 438 (2023) 114562.
- [24] M. Zhang, R. Su, Q. Zhang, L. Hu, X. Tian, Y. Chen, H. Zhou, J. Wu, Y. Tian, Ultra-bright intercellular lipids pseudo di-BODIPY probe with low molecular weight,

- high quantum yield and large two-photon action cross-sections, *Sens. Actuators B Chem.* 261 (2018) 161–168.
- [25] F. Yu, X. Jing, W. Lin, A unique amphipathic polyethylene glycol-based fluorescent probe for the visualization of lipid droplets and discrimination of living and dead cells in biological systems, *Sens. Actuators B Chem.* 302 (2020) 127207.
- [26] X. Wei, H. Zhang, Y. Sun, J. Liu, Z. Li, Engineering a lipid droplet targeting fluorescent probe with a large Stokes shift through ester substituent rotation for in vivo tumor imaging, *Analyst* 146 (2021) 495–501.
- [27] S. Guo, C. Li, L. Lian, Z. Le, Y. Ren, Y.-X. Liao, J. Shen, J.-T. Hou, Fluorescence imaging of diabetic cataract-associated lipid droplets in living cells and patient-derived tissues, *ACS Sens* 8 (2023) 3882–3891.
- [28] Y. Tang, S. Song, J. Peng, Q. Zhang, W. Lin, An ultrasensitive lipid droplet-targeted NIR emission fluorescent probe for polarity detection and its application in liver disease diagnosis, *J. Mater. Chem. B* 10 (2022) 6974–6982.
- [29] J. Sha, W. Liu, X. Zheng, Y. Guo, X. Li, H. Ren, Y. Qin, J. Wu, W. Zhang, C.-S. Lee, P. Wang, Polarity-sensitive probe for two-photon fluorescence lifetime imaging of lipid droplets in vitro and in vivo, *Anal. Chem.* 95 (2023) 15350–15356.
- [30] X. Guo, B. Tang, Q. Wu, W. Bu, F. Zhang, C. Yu, L. Jiao, E. Hao, Engineering BODIPY-based near-infrared nanoparticles with large Stokes shifts and aggregation-induced emission characteristics for organelle specific bioimaging, *J. Mater. Chem. B* 10 (2022) 5612–5623.
- [31] J. Yin, M. Peng, Y. Ma, R. Guo, W. Lin, Rational design of a lipid-droplet-polarity based fluorescent probe for potential cancer diagnosis, *Chem. Commun.* 54 (2018) 12093–12096.
- [32] S. Vuckovic, S. Song, J. Kozłowski, E. Sim, K. Burke, Density Functional Analysis: The Theory of Density-Corrected DFT, *J. Chem. Theory Comput.* 15 (2019) 6636–6646.
- [33] C. Shao, M. Grüne, M. Stolte, F. Würthner, Perylene bisimide dimer aggregates: fundamental insights into self-assembly by NMR and UV/Vis spectroscopy, *Chem. Eur. J.* 18 (2012) 13665–13677.
- [34] D. Fraher, A. Sanigorsk, N.A. Mellett, P.J. Meikle, A.J. Sinclair, Y. Gibert, Zebrafish embryonic lipidomic analysis reveals that the yolk cell is metabolically active in processing lipid, *Cell Rep.* 14 (2016) 1317–1329.
- [35] H. Heras, M.R. Gonzalez-Baró, R.J. Pollero, Lipid and fatty acid composition and energy partitioning during embryo development in the shrimp *Macrobrachium borellii*, *Lipids* 35 (2000) 645–651.
- [36] M. Hölltä-Vuori, V.T.V. Salo, L. Nyberg, C. Brackmann, A. Enejder, P. Panula, E. Ikonen, Zebrafish: gaining popularity in lipid research, *Biochem. J.* 429 (2010) 235–242.
- [37] R. Rosa, R. Calado, A.M. Andrade, L. Narciso, M.L. Nunes, Changes in amino acids and lipids during embryogenesis of European lobster, *Homarus gammarus* (Crustacea: Decapoda), *Physiol. B Biochem. Mol. Biol.* 140 (2005) 241–249.
- [38] E.S. Kaneshiro, Lipids of Paramoecium, *Lipid Res* 28 (1987) 1241–1258.
- Guangying Wang** obtained her Master degree from Northwest Normal University in 2019. She is currently working toward the Ph.D. degree in analytical chemistry with the Dalian University of Technology. Her research interest is the development of new fluorophore and fluorescence imaging.
- Qinglong Qiao** obtained his Ph.D. from Dalian University of Technology in 2017. He is currently an associate professor at the Dalian Institute of Chemical Physics, Chinese Academy of Sciences. His research interest is the development of new fluorophore, fluorescent probe designing and super-resolution fluorescence imaging.
- Ning Xu** obtained his M.S. degree from Shandong University of Technology in 2018. He is currently working toward the Ph.D. degree in Dalian University of Technology. His research interest is the development of new fluorophore and fluorescence imaging.
- Xiang Wang** obtained his B.S. degree from Southwest Medical University in 2022. He is currently working toward the Master degree in surgery with the Dalian Medical University. His research interest is the photodynamics therapy.
- Pengjun Bao** obtained his B.S. degree from Dalian University of Technology in 2020. He is currently working toward the Ph.D. degree in analytical chemistry with the Dalian Institute of Chemical Physics. His research interest is the structure-fluorescence relationship of rhodamine dyes.
- Yinchan Zhang** obtained her B.S. degree from Zhengzhou University in 2020. She is currently working toward the Ph.D. degree in Dalian Institute of Chemical Physics.
- Xiaogang Liu** received his Ph.D. in 2014 from University of Cambridge. He joined Singapore University of Technology and Design (SUTD) as an Assistant Professor in 2017. Dr. Liu Xiaogang's current research is to study the fundamental structure-property relationships of organic fluorescent dyes and sensors.
- Zhaochao Xu** was born in Qingdao, China, in 1979. He received his Ph.D. in 2006 from Dalian University of Technology under the supervision of Prof. Xuhong Qian. Subsequently, he joined Prof. Juyoung Yoon's group at Ewha Womans University as a post-doctoral researcher. Since October 2008, he was a Herchel Smith Research Fellow at University of Cambridge in Prof. David R. Spring's group. In 2011, he moved to Dalian Institute of Chemical Physics, CAS, where he is currently a Professor. His research is focusing on new fluorophore design and structure-fluorescence relationship, protein labelling and sensing, the development of fluorescent probes for the selective recognition and fluorescent imaging of biologically important species, and super-resolution fluorescent imaging.